Paul trapping of charged particles in aqueous solution

Weihua Guan[a], Sony Joseph[b], Jae Hyun Park[b], Predrag S. Krstić[b], and Mark A. Reed[a,c,1]

[a]Department of Electrical Engineering, Yale University, New Haven, CT 06520; [b]Physics Division, Oak Ridge National Laboratory, Oak Ridge, TN 37831; and [c]Applied Physics, Yale University, New Haven, CT 06520

Edited by Gregory L. Timp, University of Illinois, Urbana, IL, and accepted by the Editorial Board April 23, 2011 (received for review January 21, 2011)

We experimentally demonstrate the feasibility of an aqueous Paul trap using a proof-of-principle planar device. Radio frequency voltages are used to generate an alternating focusing/defocusing potential well in two orthogonal directions. Individual charged particles are dynamically confined into nanometer scale in space. Compared with conventional Paul traps working in frictionless vacuum, the aqueous environment associated with damping forces and thermally induced fluctuations (Brownian noise) exerts a fundamental influence on the underlying physics. We investigate the impact of these two effects on the confining dynamics, with the aim to reduce the rms value of the positional fluctuations. We find that the rms fluctuations can be modulated by adjusting the voltages and frequencies. This technique provides an alternative for the localization and control of charged particles in an aqueous environment.

ac electrophoretic effect | aqueous trapping | virtual nanopore

Trapping a single molecule or colloidal particle offers an unique opportunity to study the intrinsic individual characteristics rather than the averaged ensemble properties (1). Over the last decades, various techniques have been developed to achieve trapping in liquids, including optical tweezers (2), acoustic tweezers (3), and magnetic tweezers (4). Electrical forces for manipulating small objects in an aqueous solution include electrophoresis (EP) and dielectrophoresis (DEP) (5). Electrophoretic forces arise from the interaction of the object's fixed charge and an external electric field, whereas DEP arises from the object's polarizability in a spatially inhomogeneous electric field. To date, the electrical trapping of objects in solution has been done primarily by DEP (6, 7). Even though most macromolecules (DNA molecules, for example) suspended in aqueous solutions develop net electric charges (by either the dissociation of chemical groups or the adsorption of ions or molecules from the solution), utilization of the direct charge-field interaction to trap objects in aqueous solution has been rarely explored. It was realized five decades ago that charged particles (e.g., ions) can be trapped and confined in inhomogeneous, oscillatory electric fields. The best-known examples are quadrupole Paul traps (8), which have been used in many fields, such as mass spectrometry (9), analytical chemistry (10), and quantum information processing (11). Moreover, nanoscale Paul traps may be capable of trapping a single electron (12), ions in aqueous solutions (13), as well as a long DNA polymer (14). In contrast to the 3D Paul traps, a linear Paul trap is compatible with standard microfabrication technology and can thus be mass produced (15). Linear Paul traps confine the ions radially by a 2D rf field and transport the ions axially by an applied axial electric field (16). However, all Paul traps and the variants (11, 15, 17) experimentally realized so far have only been operated either in vacuum or in gaseous phase. An aqueous Paul trap remains an unexplored area. In fact, there are contradictory predictions whether a Paul trap is applicable in an aqueous environment (13, 17, 18).

This work serves as a first step toward realizing an aqueous Paul trap. We use a planar Paul trap device to experimentally demonstrate the feasibility of trapping charged particles in an aqueous solution, as previously predicted by molecular dynamic simulations (13). Our device functions similarly to a conventional linear Paul trap (16), with the addition of an advantageous damping term due to the fluid viscosity. We also investigate the impact of the Brownian noise on the confining dynamics, aiming to reduce the rms value of the positional fluctuations. We find that, by using finely tuned driving parameters, the rms fluctuations can be significantly modulated and minimized.

Materials and Methods

The planar aqueous Paul trap (PAPT) devices are produced by conventional microfabrication methods on an insulating SiO_2 substrate. Quadruple microelectrodes define the confinement region (Fig. 1 *A* and *B*; $2R_0$ denotes the device's physical size, which varies between 2 and 8 μm in this work). The devices are assembled with polydimethylsiloxane microfluidic chambers to form the functional devices (Fig. 1*C*). Detailed fabrication process is presented in the *SI Appendix*, section S1. The assembled devices are wire-bonded and mounted onto a printed circuit board. Voltages in the form of $\pm(U - V\cos\Omega t)$ are used to perform the trapping experiments (Fig. 1*A*). Here U is the dc voltage in series with the time-varying rf sinusoidal voltage of amplitude V and angular frequency Ω ($=2\pi f$, and f is the frequency in hertz). The carefully controlled fabrication process results in smooth electrode sidewall profiles (Fig. 1*B*). Particles in the microfluidic chamber move freely in the x-y plane but are constrained mechanically in the z direction by the chamber height (2.5 μm in this experiment, molded using SU-8 2002) (Fig. 1*C*). Future designs could incorporate an additional electric field perpendicular to the trapping field, if the particle translocation through the trap is desired.

The basic principle of the PAPT device is shown in Fig. 1 *D* and *E*. At time $t = 0$, the applied voltage creates a saddle shape potential such that positive charges will be pushed into the center of the device along the y direction but will be pulled away from the center along the x direction (Fig. 1*D*). After half an rf cycle ($t = \pi/\Omega$), the polarity of the potential is reversed and the positive charges are subject to opposite forces (Fig. 1*E*). The focusing/defocusing forces alternate between x and y directions with the applied sinusoidal voltage. If the polarity of the voltage changes fast enough, charged particles become stuck in a rapid back-and-forth motion. Note that this mechanism also works for negatively charged particles in a similar way. Because the electric field intensity is at a minimum in the trap center ($x = y = 0$), an effective pseudoforce will push the charged particles (either positively or negatively charged) toward the center, where they become confined in the x-y plane.

The motion of the charged particles is monitored by an optical microscope (Olympus BX51) and the video is taken by a high-sensitivity digital CCD camera (Olympus DP70) with the highest shutter speed as fast as 1/44,000 s (Fig. 1*F*). Video processing is performed using the National Institutes of Health ImageJ platform (see *SI Appendix*, section S2 for details).

Charged particles used to verify the working principles are polystyrene beads (Polysciences) of two diameters (0.481 ± 0.004 μm and 0.982 ± 0.013 μm). The surfaces of these particles are functionalized with carboxylate groups (-COOH). These COOH surface groups are the origin of the negative

Author contributions: W.G. and M.A.R. designed research; W.G. performed experiments; S.J., J.H.P., and P.S.K. contributed analytic tools; W.G., J.H.P., P.S.K., and M.A.R. analyzed data; and W.G. and M.A.R. wrote the paper.

The authors declare no conflict of interest.

This article is a PNAS Direct Submission. G.L.T. is a guest editor invited by the Editorial Board.

[1]To whom correspondence should be addressed. E-mail: mark.reed@yale.edu.

This article contains supporting information online at www.pnas.org/lookup/suppl/doi:10.1073/pnas.1100977108/-/DCSupplemental.

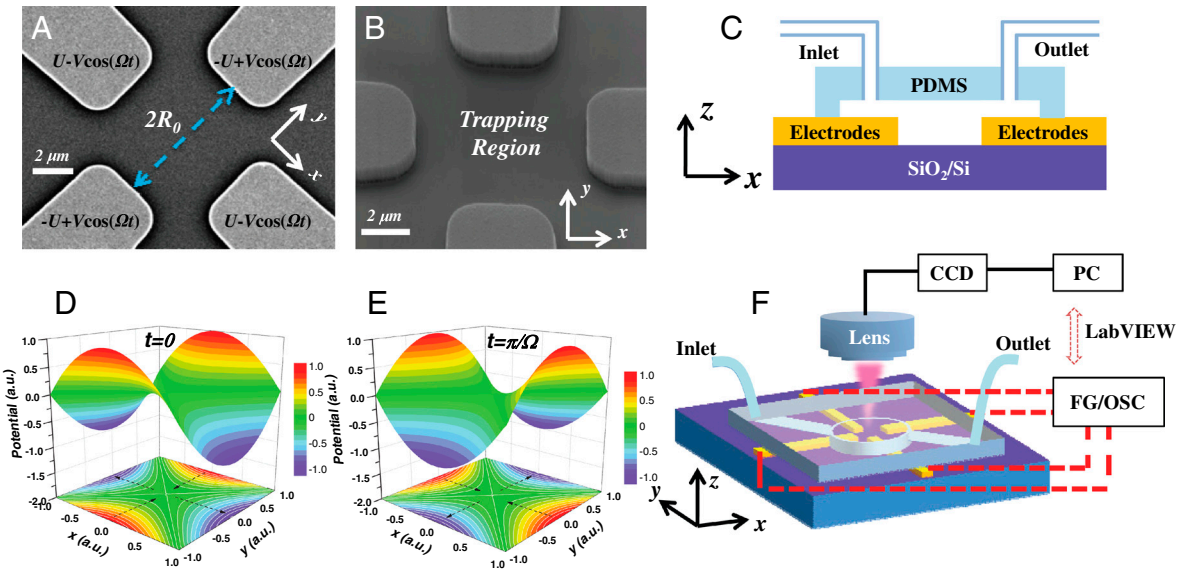

Fig. 1. PAPT devices and experimental platform. (*A*) SEM of PAPT devices before integration with a microfluidic interface. The ac/dc voltages are applied such that the potentials of any two adjacent electrodes are of same magnitude but opposite sign. The physical size of the device is denoted $2R_0$. (*B*) Finely controlled processing results in smooth sidewalls of the electrodes, which helps to minimize the stray electric fields. (*C*) Sketch of a functional device with microfluidics integrated (not drawn to scale). PDMS, polydimethylsiloxane. (*D* and *E*) Illustration of working principles for the device shown in *A* under a pure ac case ($U = 0$). The x and y axes are normalized by R_0. The z axis is normalized by V. At $t = 0$, the resulting electric forces (dashed arrows) will focus positively charged particles along the y direction and defocus them along the x direction. Half an rf period later, the potential polarity is reversed and opposite electric forces are thus generated. If the ac potential changes at the right frequency, the charged particles become stuck in this rapid back-and-forth motion. (*F*) Schematic of the experimental setup. The whole setup is built around a microscope. A LabVIEW (National Instruments) program controls the function generator (FG) to create the ac/dc voltages. The real voltage applied to the device is measured by an oscilloscope (OSC) and recorded by the same LabVIEW program. The electrical connections are through Bayonet Neill-Concelman cables (dashed lines). The videos taken by CCD are stored in personal computer (PC) memory in real time.

charges ($-COOH \rightleftarrows COO^- + H^+$). SEM reveals that all the particles have a pronounced spherical shape.

The solutions used in our experiment are repeatedly washed with deionized (DI) water (milli-Q grade, resistivity 18 MΩ · cm) to obtain a low solution conductivity. The detailed protocol of solution preparation is described in the *SI Appendix*, section S3. A lower solution conductivity is preferred for the Paul trap effect (which is an ac electrophoretic effect) to dominate over the DEP effect (see *SI Appendix*, section S4 for a detailed discussion).

Results and Discussion

Confinement. Fig. 2 presents the trapping results with PAPT devices. Inset *A* of Fig. 2 shows a typical image for a single trapped charged bead (of mean radius 490 nm). Individual particles can be stably held in the center of the device for up to 4 h (due to insignificant change over this time, we did not explore longer). Trapping mostly occurs for a single particle (instead of ensembles) due to interparticle Coulomb repulsion. The orange curve in Fig. 2 describes the time trace of the particle trajectory in the x direction when trapped under conditions of $V = 1.5$ V, $U = 0$ V, and $f = 2.5$ MHz. The blue curve depicts the Brownian motion when the trap is off (no electrical connection). We observe that the particles are not stationarily trapped but trapped with fluctuations (inset *B* of Fig. 2). Inset *C* shows the normal distribution of displacements derived from the orange trajectory in Fig. 2. A Gaussian fit yields an effective trap stiffness $k = k_B T/\delta^2$ in the x direction as 4 pN/μm (k_B is Boltzmann constant and T is the absolute temperature). The motion in the y direction shows a similar property. Note that the confinement into 32-nm range is achieved with a $2R_0 = 8$ μm device. We note that the trap stiffness of 4 pN/μm is not a characteristic value of this Paul trap. In fact, the Paul trap stiffness depends on the operation frequency, voltage, charge, and mass of the objects.

Most importantly, the rms fluctuations of the trapped particles can be tuned by externally applied voltages (U and V) and frequencies (f). Fig. 3 *A* and *B* shows the x-y positions of a trapped particle and the radial probability distributions at a fixed frequency ($f = 3$ MHz) and three different ac voltages. By adjusting the voltage, the degree of the radial confinement can be modulated. We observe a decrease of rms fluctuations with increasing the ac voltages (V) within ranges we can experimentally achieve. Fig. 3 *C* and *D* shows the x-y positions of a trapped particle and their radial probability distributions under a fixed voltage ($V = 1.2$ V) and three different frequencies. A slight decrease of rms fluctuations when increasing the frequency is visible for the data presented. However it is not necessarily true that increasing the frequency will reduce the rms fluctuations. As a matter of fact, because of the complexity of achieving an impedance match for the rf circuit, it is very difficult to maintain a fixed

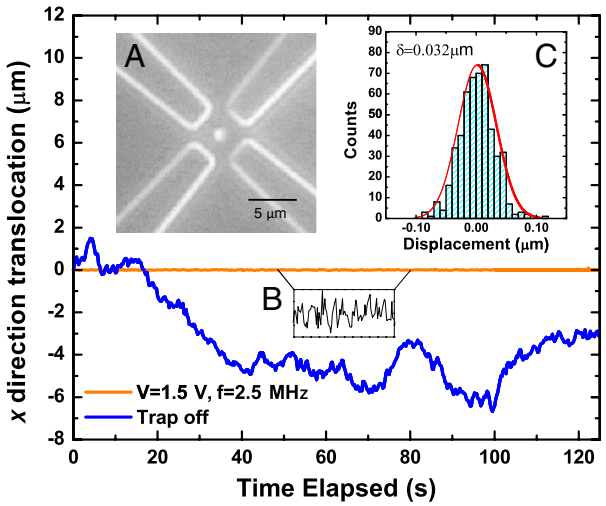

Fig. 2. Particle trajectories when the trap is on (orange line) and off (blue line) in the x direction. Inset *A* shows a snapshot of a single particle confined in the center of the device. Inset *B* shows a magnification of fluctuations. Inset *C* is the histogram of the displacements for the orange curve. A Gaussian fit yields a trap stiffness of 4 pN/μm.

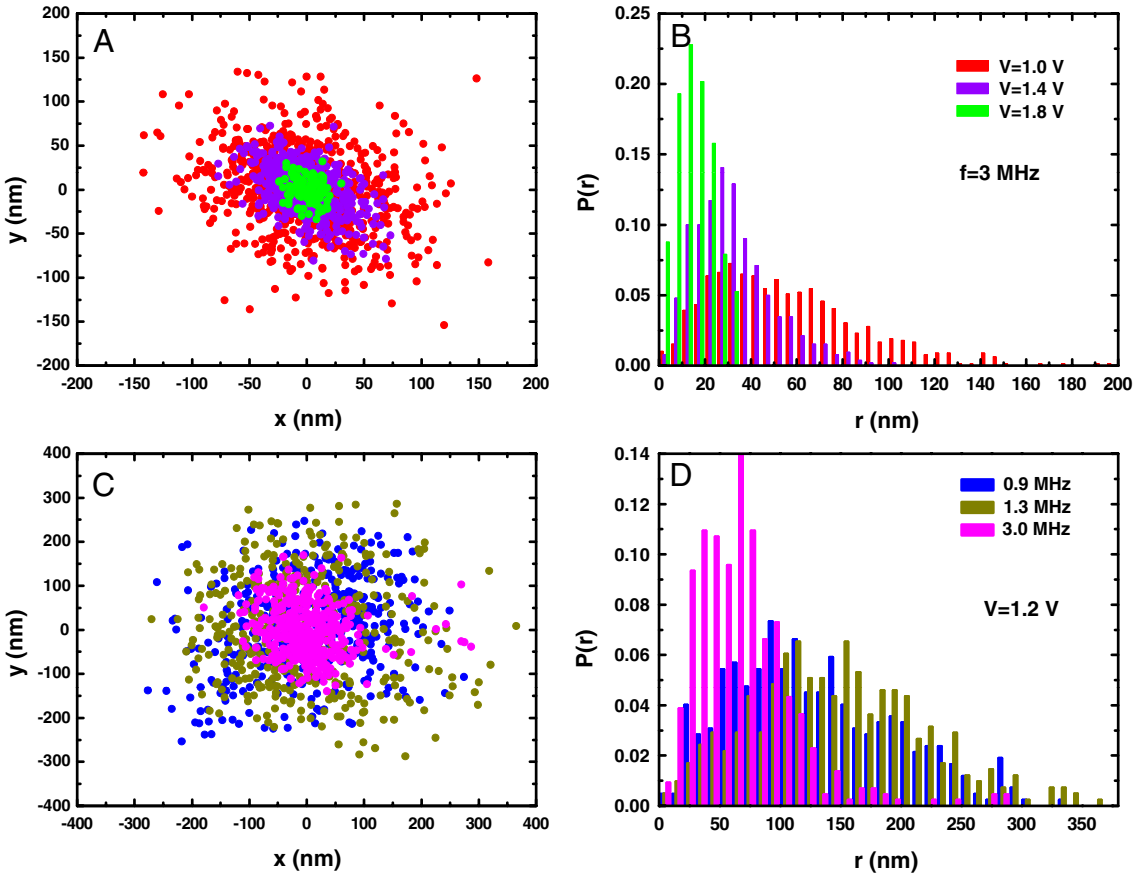

Fig. 3. Effect of the applied voltages and frequencies on the confinement of particles. Experiments are performed with 491-nm radius particles and $R_0 = 4$-μm devices. No dc voltages are applied ($U = 0$). (*A*) The *x*-*y* positions of a single particle trapped under a fixed frequency ($f = 3$ MHz) and three different voltages. (*B*) Radial probability histograms ($r = \sqrt{x^2 + y^2}$) corresponding to the datasets in *A*. $P(r)$ is defined such that $\int P(r) 2\pi r dr = 1$. (*C*) The *x*-*y* positions of a single 490-nm radius particle trapped under a fixed voltage ($V = 1.2$ V) and three different frequencies. (*D*) Radial probability histograms corresponding to the datasets in *C*.

voltage for various frequencies during the experiments. Therefore, the frequency dependence can not be decoupled from the voltage dependence (Fig. 3*A* and *B*). We do not have a conclusive trend for the frequency dependence at the current stage. Nevertheless, we can experimentally achieve a tight or loose confinement by adjusting the applied voltages and frequencies (Movie S1). In addition, we are also able to repel a confined particle from the trap and to resume confinement after the particle escapes from the trap (Movie S1).

Theoretical Modeling. Unlike the case of charged particles in a vacuum Paul trap, which has been extensively studied and described by Mathieu equations (16), the motion of charged particles in an aqueous environment is governed not only by the external electric fields but also by additional damping forces and thermally induced fluctuations (i.e., Brownian motion). The last two forces always appear together according to the fluctuation-dissipation theorem (19). This kind of system, as suggested by Arnold et al. in their study of trapping microparticles in the atmosphere near standard temperature and pressure, necessitates a stochastic approach (20).

Assuming an ideal planar rf/dc quadrupole electric potential, resulting from the applied voltages as shown in Fig. 1*A*,

$$\varphi(x,y,t) = (U - V\cos\Omega t)\frac{x^2 - y^2}{2R_0^2}, \qquad [1]$$

the motion of a homogeneous charged particle with mass M, radius r_p, and net charge Q in the presence of a stochastic force can be written as ($\vec{r}$ is the particle radial position vector in *x*-*y* plane, $\vec{r} = x\vec{i} + y\vec{j}$),

$$M\frac{d^2\vec{r}}{dt^2} = -\xi\frac{d\vec{r}}{dt} + Q(-\nabla\varphi) + \vec{N}(t). \qquad [2]$$

The three terms on the right-hand side of Eq. **2** are the damping force, the electric driving force, and the Brownian noise force, respectively. The Stokes' drag coefficient ξ can be approximated by $\xi = 6\pi\eta r_p$, where η is the dynamic viscosity of the aqueous solution. $\vec{N}(t)$ is a random force due to thermal fluctuation, with the properties $\langle\vec{N}(t)\rangle = 0$ and $\langle\vec{N}(t)\vec{N}(t+\tau)\rangle = 2k_BT\xi\delta(\tau)$, where $\delta(\tau)$ is the Dirac delta function.

Rewriting Eq. **2** into a parametric dimensionless form, the motion in the x and y direction takes the form of a Langevin equation,

$$\frac{d^2x}{d\tau^2} + b\frac{dx}{d\tau} + (a - 2q\cos 2\tau)x = g(\tau), \qquad [3a]$$

$$\frac{d^2y}{d\tau^2} + b\frac{dy}{d\tau} - (a - 2q\cos 2\tau)y = g(\tau), \qquad [3b]$$

where $\tau = \Omega t/2$ is a dimensionless scaled time, $a = 4QU/MR_0^2\Omega^2$ is the scaled dc voltage, $q = 2QV/MR_0^2\Omega^2$ is the scaled ac voltage, $b = 2\xi/M\Omega$ is the scaled damping coefficient, and $g(\tau)$ is the scaled thermal fluctuation force, following a Gaussian distribution with zero mean and standard deviation of $\sqrt{32k_BT\xi/M\Omega^2}$.

It is worth noting that the geometry of our PAPT devices is not an ideal 2D structure, which would require high aspect ratios for the four electrodes (16). However, 3D calculations (*SI Appendix*, section 6) show that the analysis will not be affected significantly as long as the particle remains within the height of the electrodes. Above the electrodes, the potential changes as if the device radius R_0 is increased. As a result, we can deal with this nonideal 2D situation by adopting an effective device radius R_0^*. Moreover, the potential profile of the PAPT device is not exactly an ideal quadruple field because of the existence of higher-order components. Taking these two effects into account, a correction factor Γ should be introduced in the expression of a and q,

$$a = \frac{4QU}{\Gamma M R_0^2 \Omega^2} \quad \text{and} \quad q = \frac{2QV}{\Gamma M R_0^2 \Omega^2}. \qquad [4]$$

The solutions of Eq. **3** will determine the dynamics of particles inside the trap. As is well known for Paul traps in vacuum [$b = 0$ and $g(\tau) = 0$], stable trapping will only occur when parameters (q,a) are within certain regions in the $q - a$ diagram (where Eq. **3** has convergent solutions) (8). If a viscous medium is present ($b > 0$, for example, air or water), the stable region in the $q - a$ diagram will not only be shifted but also be extended (21). The deterministic damped Mathieu equation without taking thermal fluctuations into consideration reads as the homogeneous part of Eq. **3** [with $g(\tau) = 0$]. With this deterministic system, the particles should settle toward the center of the device ($x = y = 0$) and eventually be trapped without moving when time $t \to \infty$ if the (q,a) parameters are inside the stability region. This prediction is, however, not true in our experiment, where positional fluctuations are observed (Fig. 2). The fluctuations of the trapped particles confirm the necessity to include the stochastic Brownian effect to study the PAPT device. The questions that arise are how this white Brownian noise affects the stability of the trapping dynamics and the rms value of the position fluctuations. We will address these two aspects in the following discussion.

Brownian Noise Effect on Trapping Stability. Zerbe et al. (22) theoretically showed that the variance of position displacement fluctuations remains bounded for (q,a) parameters that are located within the stability zones of the damped deterministic equation [Eq. **3** with $g(\tau) = 0$]. As a result, the trapping stability is solely determined by the behavior of the deterministic system and the Brownian noise would not affect the stability boundaries. The (q,a) stability region for various damping factors b can be numerically determined using Hasegawa and Uehara's method (21). It is thus very interesting to experimentally map out the stability boundary and compare it with the theoretical predictions. The principal problem here is that, unlike atomic ions, the particles are neither identical in mass nor charge. Therefore, the boundary mapping requires that all points in the stability boundary be derived from a specific single bead throughout the experiment. We are able to record each boundary point in (V,U) coordinates successfully without losing the single trapped particle by carefully adjusting the ac and dc voltages at a fixed frequency and by recognizing when the motion is on the verge of no longer being stable. Eq. **4** translates the measured boundary from (V,U) coordinates into (q,a) coordinates by using a fitting parameter $Q/\Gamma M$ (effective charge to mass ratio), where Γ is the correction factor mentioned above.

As shown in Fig. 4*A*, the resulting measured limits of the (q,a) stability boundary reproduce the theoretical calculated boundary very well. This remarkable agreement between the theoretical boundary and experimental data strongly proves that the trapping dynamics are dominated by the Paul trap mechanism, because a DEP trap would not have such a (q,a) stability boundary. The DEP forces only contribute small perturbations near the (q,a) origin (*SI Appendix*, section 7.1). Determination of boundary points

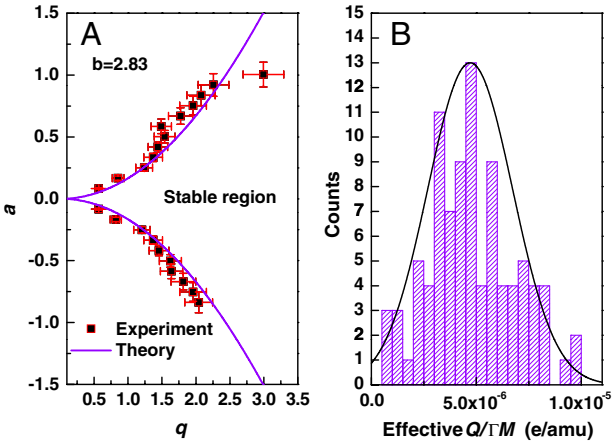

Fig. 4. (*A*) Experimental points on the boundary curves of the stability diagram as observed from a single charged particle (experiments performed with a radius of 0.491 ± 0.0065 μm at a fixed frequency $f = 2$ MHz). The solid line is the theoretically calculated stability boundary for $Q/\Gamma M = 4 \times 10^{-6}$ e per atomic mass unit. The dimensionless damping coefficient $b = 2.83$ is calculated by $b = 2\xi/M\Omega$, using known parameters. (*B*) Gaussian distribution of fitting $Q/\Gamma M$ for a total of 121 beads from the same solution. The mean value is 4.77×10^{-6} eper atomic mass unit and standard deviation is 1.95×10^{-6} e per atomic mass unit.

becomes difficult for large a values because this requires higher dc voltages, and we find experimentally that dc voltages beyond 2.2 V (corresponds to $a = 1.34$ using $Q/\Gamma M = 4 \times 10^{-6}$ e per atomic mass unit and $R_0 = 4$ μm) will result in detrimental electrochemical reactions of the metal electrodes. Surface modifications or passivations of the electrodes may improve the tolerance of high dc voltages.

By using the fitting techniques described above, we are able to evaluate the distribution of effective charge to mass ratio ($Q/\Gamma M$) for a collection of beads. We analyzed a total of 121 beads from the same suspension solution and extracted the $Q/\Gamma M$ for each single bead. Fig. 4*B* shows a Gaussian distribution for the extracted $Q/\Gamma M$, with a mean value of 4.77×10^{-6} e per atomic mass unit. This value corresponds to around 10^6 elementary charges on a single bead, which is two orders of magnitude lower than the number of carboxylate surface groups. This discrepancy may be due to the partial dissociation of carboxylate groups in solution and the charge renormalization effect (23).

Brownian Noise Effect on rms Fluctuations. Although the serial dc voltages (U) can be used to tune the trapping stability and thus the dynamics in PAPT devices (Fig. 4*A*), a pure ac field ($U = 0$) is experimentally favorable due to the obvious advantages of an ac over a dc electric field in solution. In particular, electroosmosis flow does not develop in the bulk, and electrochemical reactions can be avoided. Thermal convection can also be suppressed because the heating effect of an ac field is less (24). As a result, ac fields are of more practical interest in the context of aqueous solutions.

The rms fluctuation in the x and y directions for the ac only case ($a = 0$) can be expressed as (25),

$$\sqrt{\langle x^2 \rangle} = \sqrt{\langle y^2 \rangle} = \Theta I(b,q), \qquad [5]$$

where $\Theta = \sqrt{16 k_B T \xi / M^2 \Omega^3}$ and $I(b,q)$ is a function of dimensionless parameters b and q. The rms fluctuations as a function of applied ac voltages (V) at a fixed frequency ($f = 2$ MHz) observed in the experiment is given in Fig. 5. Because $I(b,q)$ can be approximated as $I(b,q) = \sqrt{(4 + b^2)/4bq^2}$ for small q (20) (note that the working parameter b and maximum possible q are calculated to be 2.83 and 0.604, respectively), the rms

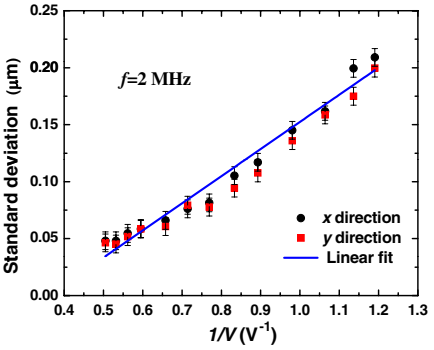

Fig. 5. Dependence of the standard deviation of position fluctuations of trapped bead on ac voltage at fixed frequency (2 MHz). The reduced χ^2 value for the linear fitting is calculated as 1.4.

fluctuations thus have the dependence on the ac voltage as $\sqrt{\langle x^2\rangle} = \sqrt{\langle y^2\rangle} \propto 1/q \propto 1/V$ for a fixed frequency (fixed damping factor b) in small q region. The linear fitting curve in Fig. 5 demonstrates a remarkable agreement with the predicted linear dependence of rms fluctuations on $1/V$. We perform this experiment under several frequency conditions and all of them show the same linear dependence (*SI Appendix*, section 8). This dependence is intuitively correct (stronger field gives a tighter trap). However, it is not necessarily true for the whole ac voltage range. Theoretical studies showed that there always exists a minimal rms fluctuation if proper working parameters q are chosen within the stability region (25). By taking the experimental parameters as $f = 2$ MHz, $Q/\Gamma M = 4 \times 10^{-6}$ e per atomic mass unit, and $b = 2.83$, we can calculate that the minimal rms fluctuations corresponds to $q = 2.78$ and $V = 9$ V. This ac voltage is beyond our instrument's ability ($V_{\max} = 5$ V) and therefore we only experimentally observe a decrease of rms fluctuations when increasing ac voltages are within ranges we can achieve (Fig. 3 *A* and *B*).

The rms fluctuation dependence on the driving parameters when $a = 0$ is theoretically studied in several works (22, 25–27). The magnitude of the minimal fluctuation (which determines the size of a virtual nanopore) can be expressed as $\sqrt{8k_BT/M\Omega^2}$, which is dependent only on the environment temperature T, the particle mass M, and the tunable working frequency Ω. This minimal fluctuation will happen when $q = 0.751\sqrt{4+b^2}$ (25). The existence of such a minimum in the positional fluctuation of the stochastically confined motion is of considerable importance because one can significantly reduce the thermal noise effect on the positional uncertainty of the motion. It is noteworthy that the operating parameters (q,a) must be inside of the stability region to achieve this minimal fluctuation. The minimal fluctuation for the particle shown in Fig. 5 would be 0.63 nm (with $M = 520$ fg and working frequency $f = 2$ MHz). It is apparent that higher frequency can be adopted to suppress the positional uncertainty to the greatest extent for the reduced M, if the parameters q, a, and b are kept within the stability region. For example, for a 1,000-bp dsDNA (650 Da/bp, charge to mass ratio 3×10^{-3} e per atomic mass unit), when the working frequency is increased to 442 MHz, the minimal achievable fluctuation is around 2 nm (close to the size of a physical nanopore; refs. 28–30). By careful rf circuit design, this frequency could be experimentally achievable. The practical limits of the confinement is determined by the highest frequency that can be applied without causing detrimental heating or device damage.

Conclusions

In summary, we experimentally demonstrate the feasibility of a Paul-trap-type planar device working in aqueous solutions. An oscillating quadrupole electric field generates a pseudopotential well and the charged particles are dynamically confined to a nanometer scale region, whose size can be externally tuned by driving parameters (voltages and frequencies). This technique opens up the possibility of spatially controlling the object in a liquid environment and can lead to lab-on-a-chip systems controlling single molecules that often appear charged when submerged in water. Further investigations such as the impact of variation of the solution's ionic composition, concentrations, and pH on the trapping performance are needed for a better understanding for biomolecular applications.

ACKNOWLEDGMENTS. This research was supported by the US National Human Genome Research Institute of the National Institutes of Health under Grant 1R21HG004764-01. P.S.K. acknowledges partial support of the US Department of Energy, through Oak Ridge National Laboratory (ORNL). S.J. and J.H.P. acknowledge support through ORNL Postdoctoral Program, administered by Oak Ridge Institute for Science and Education.

1. Goldsmith RH, Moerner WE (2010) Watching conformational and photodynamics of single fluorescent proteins in solution. *Nat Chem* 2:179–186.
2. Ashkin A, Dziedzic JM, Yamane T (1987) Optical trapping and manipulation of single cells using infrared-laser beams. *Nature* 330:769–771.
3. Wu JR (1991) Acoustical tweezers. *J Acoust Soc Am* 89:2140–2143.
4. Gosse C, Croquette V (2002) Magnetic tweezers: Micromanipulation and force measurement at the molecular level. *Biophys J* 82:3314–3329.
5. Voldman J (2006) Electrical forces for microscale cell manipulation. *Annu Rev Biomed Eng* 8:425–454.
6. Hughes MP, Morgan H (1998) Dielectrophoretic trapping of single sub-micrometre scale bioparticles. *J Phys D Appl Phys* 31:2205–2210.
7. Chiou PY, Ohta AT, Wu MC (2005) Massively parallel manipulation of single cells and microparticles using optical images. *Nature* 436:370–372.
8. Paul W (1990) Electromagnetic traps for charged and neutral particles. *Rev Mod Phys* 62:531–540.
9. March RE (1997) An introduction to quadrupole ion trap mass spectrometry. *J Mass Spectrom* 32:351–369.
10. Chang HC (2009) Ultrahigh-mass mass spectrometry of single biomolecules and bioparticles. *Annu Rev Anal Chem* 2:169–185.
11. Stick D, et al. (2006) Ion trap in a semiconductor chip. *Nat Phys* 2:36–39.
12. Segal D, Shapiro M (2006) Nanoscale paul trapping of a single electron. *Nano Lett* 6:1622–1626.
13. Zhao X, Krstic PS (2008) A molecular dynamics simulation study on trapping ions in a nanoscale paul trap. *Nanotechnology* 19:195702.
14. Joseph S, Guan WH, Reed MA, Krstic PS (2010) A long DNA segment in a linear nanoscale paul trap. *Nanotechnology* 21:015103.
15. Cruz D, et al. (2007) Design, microfabrication, and analysis of micrometer-sized cylindrical ion trap arrays. *Rev Sci Instrum* 78:015107.
16. Douglas DJ, Frank AJ, Mao DM (2005) Linear ion traps in mass spectrometry. *Mass Spectrom Rev* 24:1–29.
17. Allison EE, Kendall BRF (1996) Cubic electrodynamic levitation trap with transparent electrodes. *Rev Sci Instrum* 67:3806–3812.
18. Holzel R, Calander N, Chiragwandi Z, Willander M, Bier FF (2005) Trapping single molecules by dielectrophoresis. *Phys Rev Lett* 95:128102.
19. Kubo R (1966) The fluctuation-dissipation theorem. *Rep Prog Phys* 29:255–284.
20. Arnold S, Folan LM, Korn A (1993) Optimal long term imaging of a charged microparticle at the center of a paul trap in an atmosphere near standard temperature and pressure: Experiment and stochastic model. *J Appl Phys* 74:4291–4297.
21. Hasegawa T, Uekara K (1995) Dynamics of a single-particle in a Paul trap in the presence of the damping force. *Appl Phys B* 61:159–163.
22. Zerbe C, Jung P, Hanggi P (1994) Brownian parametric oscillators. *Phys Rev E Stat Nonlin Soft Matter Phys* 49:3626–3635.
23. Alexander S, et al. (1984) Charge renormalization, osmotic-pressure, and bulk modulus of colloidal crystals—theory. *J Chem Phys* 80:5776–5781.
24. Dukhin AS, Dukhin SS (2005) Aperiodic capillary electrophoresis method using an alternating current electric field for separation of macromolecules. *Electrophoresis* 26:2149–2153.
25. Izmailov AF, Arnold S, Holler S, Myerson AS (1995) Microparticle driven by parametric and random forces—theory and experiment. *Phys Rev E Stat Nonlin Soft Matter Phys* 52:1325–1332.
26. Blatt R, Zoller P, Holzmuller G, Siemers I (1986) Brownian motion of a parametric oscillator: A model for ion confinement in radio frequency traps. *Z Phys D Atom Mol Cl* 4:121–126.
27. Tashiro T, Morita A (2007) Brownian motion under a time-dependent periodic potential proportional to the square of the position of a particle and classical fluctuation squeezing. *Phys A* 377:401–411.
28. Li JL, Gershow M, Stein D, Brandin E, Golovchenko JA (2003) DNA molecules and configurations in a solid-state nanopore microscope. *Nat Mater* 2:611–615.
29. Storm AJ, Chen JH, Ling XS, Zandbergen HW, Dekker C (2003) Fabrication of solid-state nanopores with single-nanometre precision. *Nat Mater* 2:537–540.
30. Branton D, et al. (2008) The potential and challenges of nanopore sequencing. *Nat Biotechnol* 26:1146–1153.

Supplementary Information for

Paul Trapping of Charged Particles in Aqueous Solution

Weihua Guan,[1] Sony Joseph,[2] Jae Hyun Park,[2] Predrag S. Krstić,[2] and Mark A. Reed[1,3,*]

[1]*Department of Electrical Engineering, Yale University, New Haven, Connecticut 06520*

[2]*Physics Division, Oak Ridge National Laboratory, Oak Ridge, Tennessee 37831*

[3]*Applied Physics, Yale University, New Haven, Connecticut 06520*

[*] Electronic Address: mark.reed@yale.edu

CONTENTS

S1. DEVICE FABRICATION

Our planar quadrupole trapping devices are fabricated on a SiO_2/Si wafer (Fig. S1a). The insulating SiO_2 layer has a thickness of 3 μm which is thermally grown. LOR 5A resist (Microchem Corp) is spined on the substrate at a speed of 3000 rmp for 1 min, followed by baking at 175 °C for 5 min on the hotplate. Another layer of positive photoresist S1808 (Shipley) is then spun on top of the baked LOR. Then a standard UV lithography and developing process is applied to pattern the bi-layer structure. 20-nm-thick Cr and 300-nm-thick Au is e-beam evaporated at the speed of 3 $\mathring{A}/s$. The whole wafer is thereafter immersed into the N-Methylpyrrolidone (NMP) solution heated at 60°C to remove the bi-layer photoresist. Finally, the wafer is diced and is ready to be integrated with the microfluidic chamber. The microfluidic chamber is formed by poly(dimethylsiloxane) (PDMS) using SU-8 as a molding master (Fig. S1c and d). The detailed protocols can be found in ref. [1]. Oxygen plasma treatment was used to permanently bond the PDMS to the device surface and form an anti-evaporation microfluidic channel(Fig. S1e). An inlet and an outlet were punched through before assembling(Fig. S1f). Once the device was assembled, it could be repeatedly used for a long time.

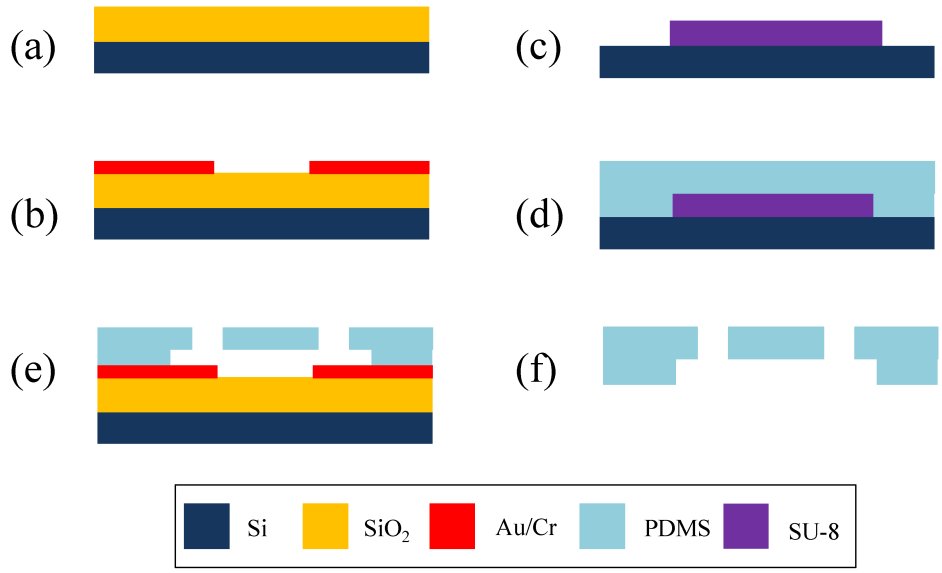

Figure S1. Schematic device fabrication flow

S2. VIDEO PROCESSING METHOD

We use a particle tracking algorithm that has been described in detail elsewhere [2] to extract the motion fluctuations. The videos are taken by a high-sensitivity digital CCD camera (Olympus DP70) with the highest shutter speed as fast as 1/44000 s. Videos are decomposed into frame sequences using the software VirtualDub (`http://www.virtualdub.org/`). The particle tracking is then carried out in NIH ImageJ platform (`http://rsb.info.nih.gov/ij/`) with a particle tracking plugin tool developed by G. Levy (`https://weeman.inf.ethz.ch/ParticleTracker/`). Fig. S2 illustrates the trajectory extraction process.

However, video based position extraction method does not measure the instantaneous particle position and has a problem of 'motion blur', which results from time-averaging a signal over a finite integration time (shuttle time or acquisition time) [3]. This will lead to the underestimation of the real variance. Wong *et al.* showed both theoretically and experimentally that the relation between the measured variance $Var(X_m)$ and the real variance $Var(X_r)$ can be linked by motion blur correction function $S(\alpha)$ [3], $Var(X_r) = Var(X_m)/S(\alpha)$, where $S(\alpha) = \frac{2}{\alpha} - \frac{2}{\alpha^2}(1 - e^{-\alpha})$, and α is a dimensionless parameter, defined by expressing the exposure time W in unit of the trap relaxation time τ, i.e. $\alpha = W/\tau$.

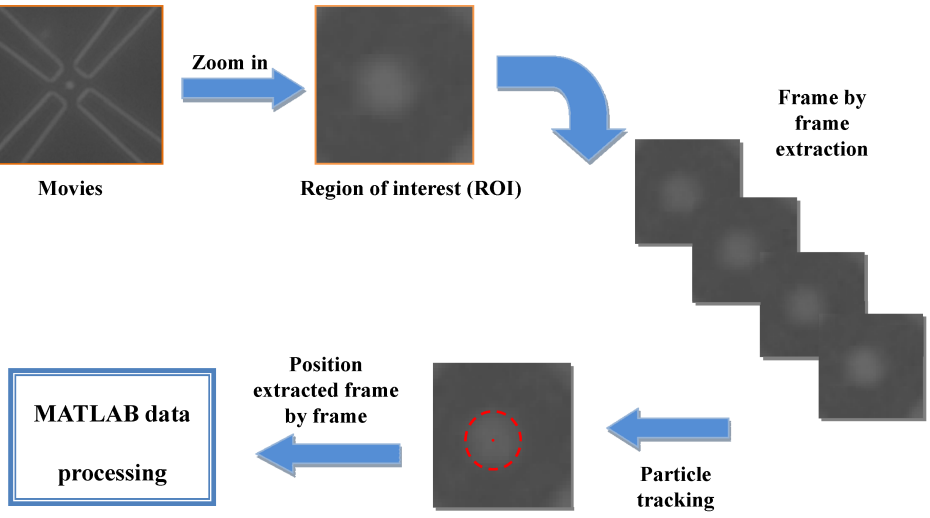

Figure S2. Illustration of trajectory extraction method

As for the position variance extraction experiments, we set the shutter speed as 1/80 s and used a 100× objective, leading to an on-screen magnification of 125 nm/pixel. The recording

frame rate is 8 fps. We estimate the relaxation time in the experiment as $\tau = \xi/k \sim 1ms$ (where $\xi = 6\pi\eta r$, the Stokes' drag coefficient). As a result, the motion blur correction function value $S(\alpha)|_{\alpha=12.5} = 0.1472$. Therefore, the real variance $Var(X_r)$ is corrected as, $Var(X_r) = 6.79 \times Var(X_m)$, or in terms of standard deviation, $Std(X_r) = 2.6 \times Std(X_m)$

S3. SOLUTION PREPARATION

The solution used in the experiment was prepared by the following steps:

(1) The beads were firstly diluted to a density of $\sim 10^6$ particle/mL by deionized (DI) water (milli-Q grade, resistivity 18 $M\Omega \cdot cm$), in order to eliminate the particle-particle interactions during the experiment.

(2) In order to thoroughly remove the residual ions from the stock solution, the beads prepared in step 1 were washed five times in DI water by centrifuging the beads in a 10 mL tube at 13500 G for 10 min, re-suspending in DI water each time.

The prepared solution in the 10 mL tube was extracted and then pumped into the microfluidic chamber. The conductivity of the fresh suspension solution in the 10 mL tube (exposed to air) is measured as 0.1 $\mu S/cm$ (EC 215 Multi-range Conductivity Meter, Hanna Instruments) and this slowly goes up to maximum 2.0 $\mu S/cm$ during the course of an experiment (due to the absorption of ambient gas). This measured conductivity variation sets the lower and upper bound for the solution inside the microfluidic chamber. In fact, since the microfluidic channels are not directly exposed to air, little change of the solution conductivity inside the trap chamber is expected. Since the solution conductivity directly affects the effective charge of the particle (see Section S4), long-term measurements were carried out on a single trapped particle to investigate the drift of solution conductivity. We find that we can stably trap particles for a minimum of 4 hours (we did not explore longer), and over this time the trap stiffness ($k = k_B T/\delta^2$) only changed by $< 3\%$ (Fig. S3), indicating a stable solution conductivity during the 4-hour period.

S4. EFFECT OF SOLUTION CONDUCTIVITY

Maintaining a low solution conductivity is critical to observe the Paul trapping effects (instead of DEP effects) for our current devices. Notice that the charge we used in the

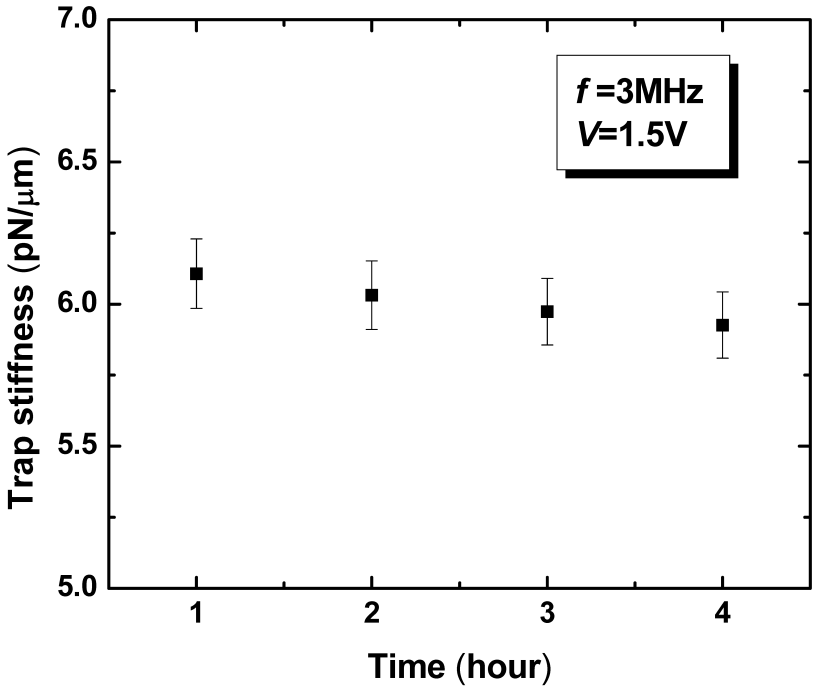

Figure S3. Long-term trap stiffness for a single trapped bead (particle radius 491 nm and device size R_0=4 μm).

derivations in the main text is the effective charge rather than the bare charge. A charged surface in contact with a conductive liquid creates an induced electric double layer (EDL). A significant fraction of the particle's charge is neutralized by the strongly bounded counterions in the Stern layer. The charged particle plus the thin Stern layer is further screened by diffusive counterions within a characteristic Debye length λ_D. To determine the effective charge Q_{eff}, we look at the motion of charged particles, which is induced by electrostatic forces, friction, and electrophoretic retardation forces. Among them, the electrophoretic retardation force originates from the delayed response of the surrounding ionic atmosphere to the motion of a charged particle. The electrophoretic mobility including this retardation effect can be described by Henry's formula [4],

$$\mu_E = \frac{2}{3}\frac{\varepsilon\zeta}{\eta} f(\alpha) \tag{S1}$$

where $\alpha = a/\lambda_D$ is the ratio of particle radius to the Debye length of the electrolyte solution, ε is the dielectric constant of the electrolyte, ζ is the zeta-potential, and η is viscosity of the solution. Ohshima *et al.* [5] showed that $f(\alpha)$ is a monotonic increasing function that

varies from 1 to 3/2. Since ζ-potential can be expressed in Debye-Hückel form [6],

$$\zeta = \frac{Q_{bare}}{4\pi\varepsilon a\left(1 + a/\lambda_D\right)} \tag{S2}$$

where Q_{bare} is the bare charge of particle. The electrophoretic mobility μ_E can be rewritten as,

$$\mu_E = \frac{Q_{bare}}{6\pi\eta a\left(1 + a/\lambda_D\right)} f\left(\frac{a}{\lambda_D}\right) \tag{S3}$$

The effective charge of particle can thus be estimated as,

$$Q_{eff} = \frac{f\left(a/\lambda_D\right)}{\left(1 + a/\lambda_D\right)} Q_{bare} \tag{S4}$$

At a high ionic concentration c, the Debye length ($\lambda_D \sim c^{-1/2}$) becomes very small, as a result, $a/\lambda_D \gg 1$ and $f\left(a/\lambda_D\right) \to 3/2$. Therefore, $Q_{eff} \approx \frac{3}{2}\frac{\lambda_D}{a} Q_{bare} \ll Q_{bare}$. The effective charge is greatly reduced in salt solutions. However, a significant amount of charge of the particle is required for Paul trap to function (Paul trap would not work with neutral particles). For most DEP trapping experiments reported, high salt concentrations were added to adjust the conductivity of the suspension medium [7–11]. Therefore the Paul trap effects can not be seen easily in these experiments. In contrast, it is easy to see that $Q_{eff} \to Q_{bare}$ when $a \to 0$ and/or $\lambda_D \to \infty$. This will happen for ultrasmall particles or very low ionic concentrations.

S5. MOVIE ILLUSTRATIONS

The affiliated video shows typical dynamics for four basic operations.

(i) Trapping with small fluctuations.

(ii) Trapping with large fluctuations.

(iii) Unstable trapping region, ejection.

(iv) Resuming trapping.

Table SI summarizes the working conditions for each part of the video. It is worth noting that for the two particles in part (iv), one particle is leaving while the other is trapped. This is believed to be due to the inter-particle coulomb repulsion. We observe in the experiment that the trapping mostly occurred for single beads, though up to 4 beads trapped simultaneously are also occasionally observed.

TABLE SI. Working parameters for each part in the video [a,b]

Video part	RF voltage (V)	DC voltage (V)	Frequency (MHz)	b	q	a
i	1.72	0	3	1.89	0.2727	0
ii	0.92	0	3	1.89	0.1458	0
iii	0.68	0	3	1.89	0.1078	0
iv	1.84	0	3	1.89	0.2917	0

[a] The device size is $2R_0$=7.4 μm, bead radius is r_p=490 nm.

[b] b, q and a parameters are calculated by using $Q/\Gamma M = 4.77 \times 10^{-6}$ e/amu.

S6. CALCULATION OF THE ELECTRIC POTENTIAL FOR THE REAL PLANAR DEVICE GEOMETRY

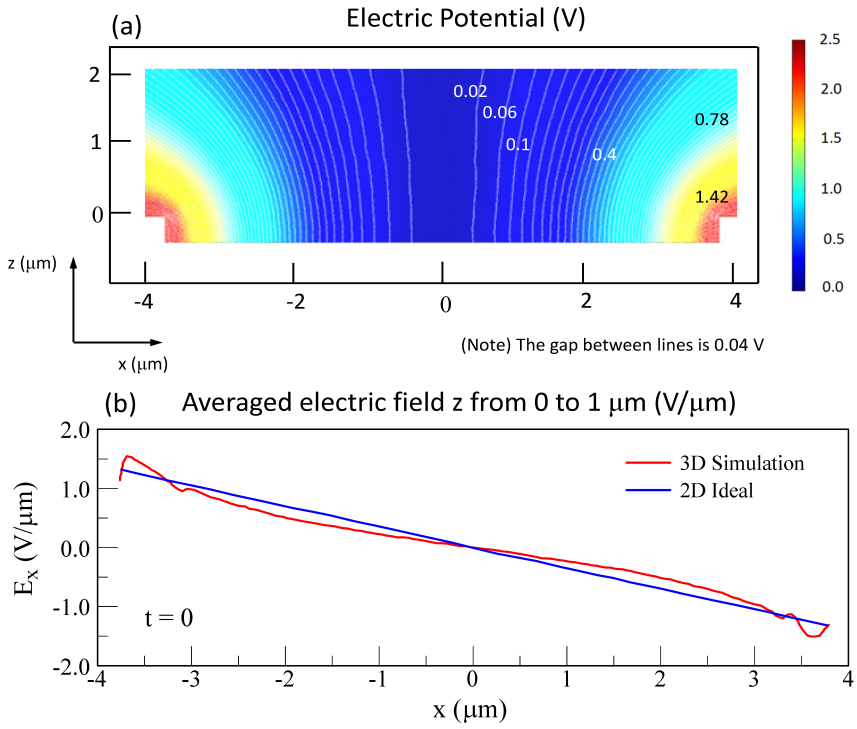

Figure S4. (a) The electric potential distribution in $x-z$ plane calculated for the real 3D geometry. (b) Comparison of the x-component potential for the real device with finite height (averaged over z from 0 to 1 μm) and an ideal 2D device at one instant of time (t=0).

We numerically calculated (using COMSOL software package, `http://www.comsol.com`,

COMSOL Multiphysics Ouick Start and Quick Reference, COMSOL LAB.)) a 3D potential distribution in the trap for an AC potential of 5 Vpp (peak to peak voltage) on the electrodes for the device geometry extracted from a SEM image. Fig. S4(a) shows the potential profile in a cross section ($x-z$ plane) for this realistic geometry. From the result it is seen that as long as the spherical particle remains within the height of the electrodes, it is close to an ideal 2D trap. Above the electrodes, the potential changes as if the device size is increased. The lines around z= 2 μm (chamber height 2.5 μm) shows where along the z axis the microfluidic chamber walls restrict the motion of the particle. Fig. S4(b) is a comparison of the x-component potential for the real device with finite height (averaged over z from 0 to 1 μm) and an ideal 2D device at one instant of time (t=0).

S7. CONSIDERATION OF DEP TRAPPING MECHANISM

S7.1. Theoretical calculation of DEP impact on stability diagram

Besides the direct interaction of the particle's net charges and the electric field (Paul trap), there are also interactions between the particle's polarizability and the electric field. Here we consider the impact of dielectrophoretic (DEP) forces on the $q-a$ stability diagram. The dimensionless form of the equation of motion in x-direction of a charged particle of radius a in the Paul trap defined by parameters a and q (Eq. [3] of the main text), with damping defined by factor b, in presence of DEP forces, can be written as

$$\frac{d^2x}{d\tau^2}+b\frac{dx}{d\tau}+[a+\alpha_m K(\Omega)(aU+qV)-2q(1+2\alpha_m K(\Omega)U)\cos 2\tau+\alpha_m K(\Omega)qV\cos 4\tau]=0 \quad \text{(S5)}$$

where $\alpha_m = 4\pi a^3\varepsilon_m/QR_0^2$, and $K(\Omega)$ is the Clausius-Mossotti factor. It is easy to see that the expression above is reduced to homogeneous part of Eq. [3] in the main text when $K(\Omega)$=0 (without DEP effect).

We consider two extreme cases of DEP, the one with positive $K(\Omega)$=1 (positive DEP, pDEP), and the one with $K(\Omega) = -1/2$ (negative DEP, nDEP). We treat the above equation numerically, and find that the effect of DEP is significant only for extremely small q and a factors of Paul trap (for example, small charges of the particle). The stability diagram (solid line) from Fig. 3 in the main text is shown in Fig. S5 by solid blue line. DEP corrections only contribute a small perturbation near the $q-a$ origin ($q < 0.01$), far below the region

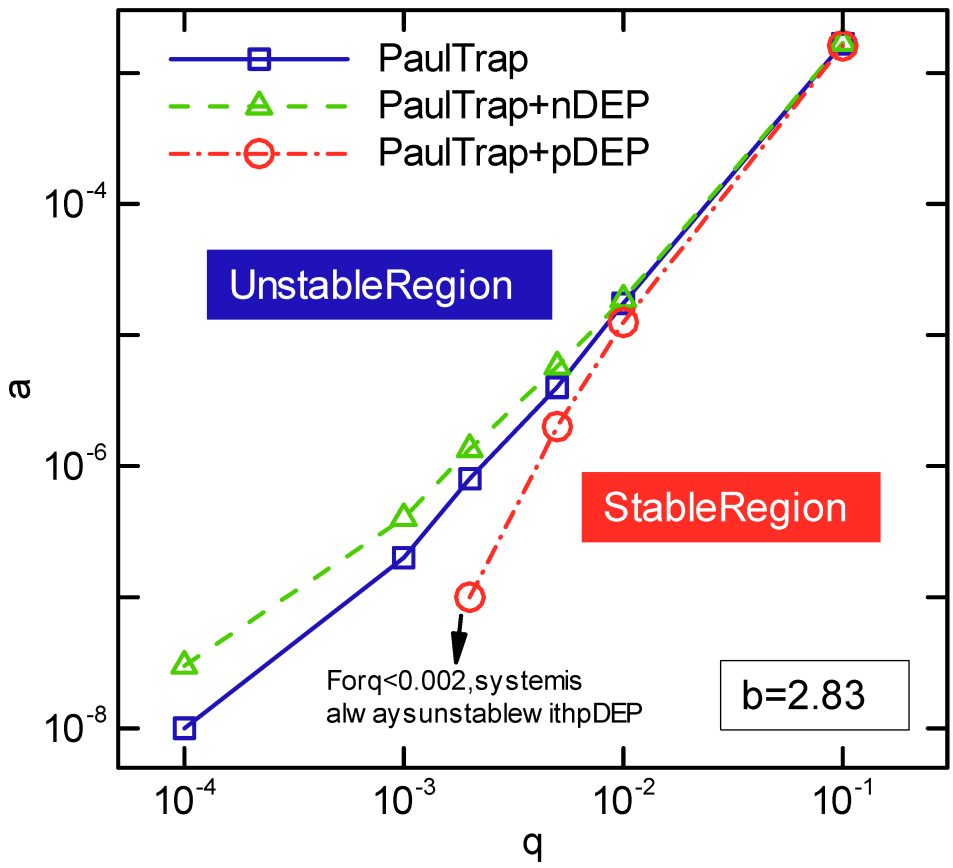

Figure S5. Magnified $q - a$ stability diagram near origin

of experimental interest ($q > 0.1$). The impact of DEP on the stability is negligible for the parameters of the Paul trap used in the present study.

S7.2. Particle size dependence experiment

The time averaged DEP force can be estimated as $\langle F_{dep} \rangle = \pi \varepsilon_m a^3 Re[K(\omega)] \nabla E_0^2(\vec{r})$. It scales with the particle volume ($\sim a^3$). Therefore, the DEP trap stiffness will decrease as a function of particle volume. On the contrary, time averaged Paul trap force can be estimated by $\langle F_{pt} \rangle = Q^2 \nabla E_0^2(\vec{r})/(4M\Omega^2(1 + (\xi/M\Omega)^2))$. Instead of a simple dependence on the particle volume, the Paul trap stiffness depends on the charge Q and mass M in a complex way. Measurements of the trap stiffness as a function of the particle size reveal whether the trapping mechanism in our experiment is dominated by DEP effect or Paul trap effect.

We used the polystyrene beads with radius ranging from 240 nm to 1.5 μm. All of these beads are surface functionalized with carboxylate surface groups. Their sizes are well characterized while the surface charge density is undetermined. The surface charges do not necessarily scale with the surface area of the particle. The suspension solution is thoroughly washed using the same procedure described above. All the trap stiffness are extracted under the condition of V=1.5 V, U= 0 V, and f=2.5 MHz, using the device with the same size (8 μm between electrode tips). Fig. S6 shows the measured trap stiffness as a function of the particle radius. As is shown, the trap stiffness does not scale with the particle volume ($\sim a^3$). In fact, when the particle radius reduces from 0.491 μm to 0.24 μm, the trap stiffness increases from 4 pN/μm to 15.2 pN/μm. This strongly proves that the trapping mechanism is not due to the DEP effect, as one would expect a decrease of trap stiffness when decreasing the particle size. We note that the irregular dependence of the trap stiffness on the particle radius in Fig. S6 comes from the irregular Q/M ratio for different particles.

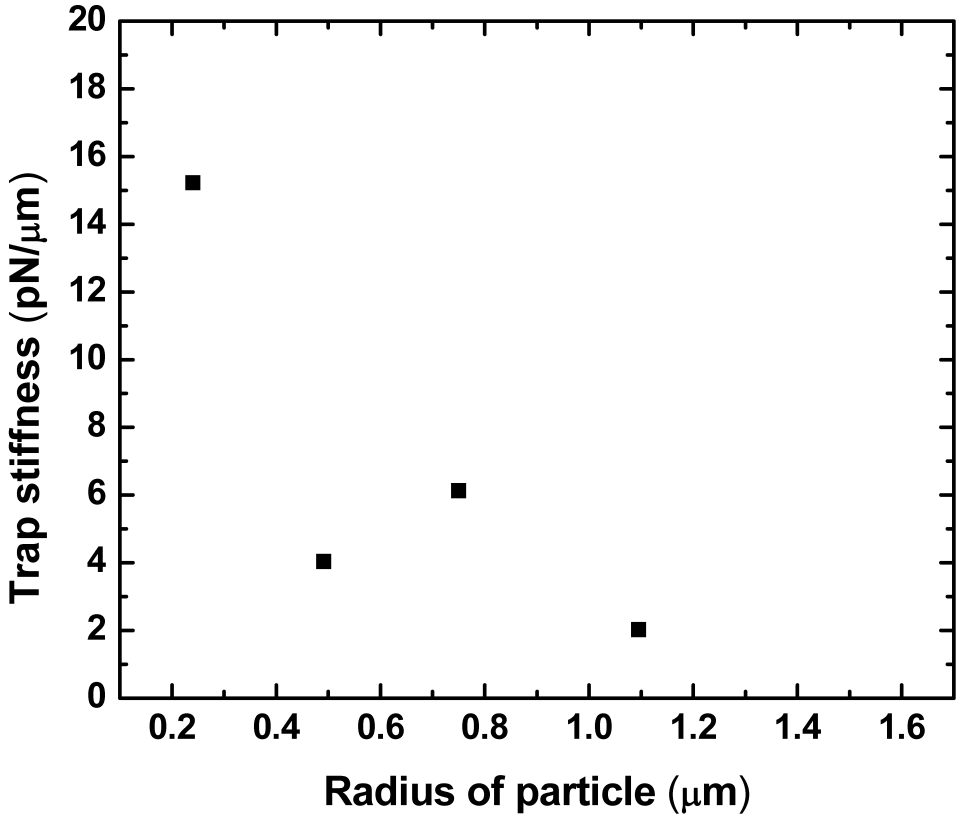

Figure S6. Trap stiffness as a function of the particle radius

S7.3. Frequency dependence experiment

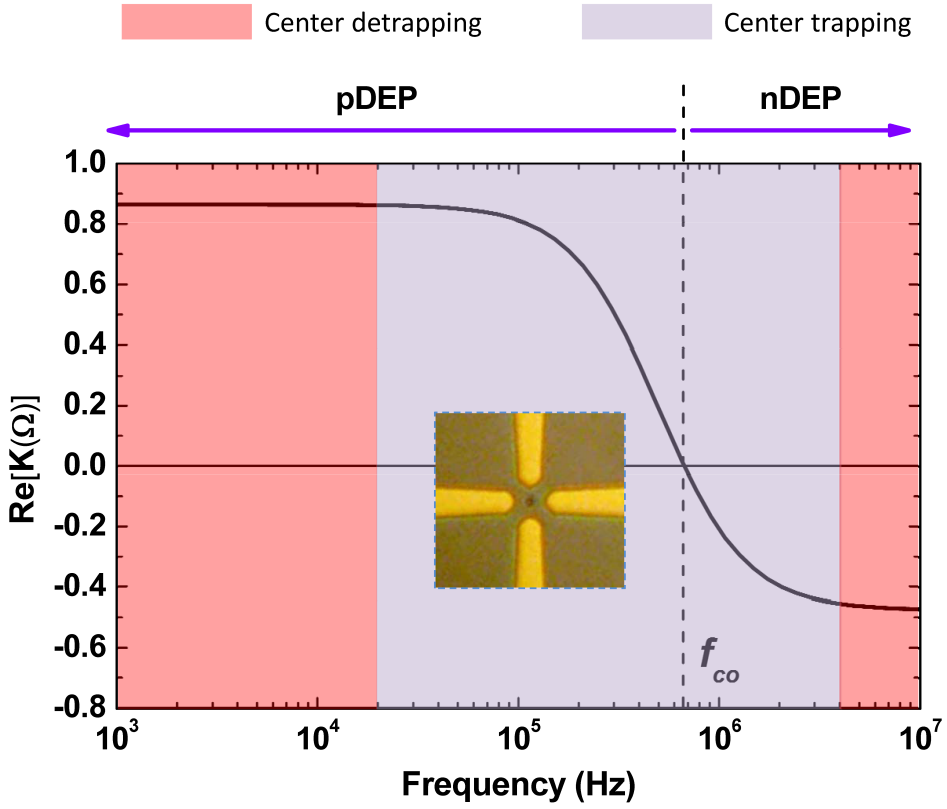

Figure S7. Particle can be trapped in the center of the device (local electric field minima) even when the operation frequency is in the positive DEP region.

Both the Paul trap and DEP effects are frequency dependent, but in a very different way. For DEP effect, the sign associated with the real part of Clausius-Mossotti (CM) factor (Re[K(ω)], which is frequency dependent) dictates the behavior of the particle [12]. For Re[K(ω)]>0, particles will be directed toward a local electric field maxima (positive DEP, pDEP), while for Re[K(ω)]<0, particle is attracted to a local electric field minima (negative DEP, nDEP). In other word, nDEP drags the particle to the center of the device while pDEP pushes the particle out of the device center. The frequency that produces a change from pDEP to nDEP is referred to as the crossover frequency f_{co} (Hz) and is given by $(1/2\pi)[(\sigma_p - \sigma_m)(\sigma_p + 2\sigma_m)/(\epsilon_m - \epsilon_p)(\epsilon_p + 2\epsilon_m)]^{1/2}$, where σ and ϵ are the conductivity and permittivity, respectively, with p and m denoting the particle and medium.Note that this crossover frequency theory is well supported by experiments [10]. For a Paul trap, the

particle confinement to the center of the trap is determined by if the $a = 4QU/MR_0^2\Omega^2$and $q = 2QV/MR_0^2\Omega^2$ parameters are within the stability region or not. It is because of this frequency dependence that we can experimentally map out the stability diagram for Paul trap (Figure 4a in main text). DEP trap would not have the (q,a) stability boundary. To more convincingly rule out the DEP effect as the trapping mechanism in the considered region of the trap parameters, we carried out the following frequency dependence experiment. Using the suspension of the low conductivity solution (prepared by the same procedure described in Section S3), we measured the solution conductivity as $\sigma_m = 2\mu S/cm$. $\sigma_p = 40\mu S/cm$(by taking into account the surface conductance). With $\varepsilon_p = 2.55\varepsilon_0$ and $\varepsilon_m = 78\varepsilon_0$, we calculate the crossover frequency frequency as f_{co}=670 KHz. Therefore, the particle will undergo a pDEP force and should be kicked out of the device center when f_{co} <670 KHz. In our experiment, the bead can be trapped in the center of the device even when the frequency is ramped down to 20 KHz due to Paul trapping (Fig. S7). Therefore, DEP effect is not a dominant mechanism. It is the Coulomb interaction of the particle charge and the Paul trap quadrupole oscillating field, together with the damping (friction) forces of the water that confine the particle toward the trap center even when the particle is subject to a pDEP force, which tends to push the particle out of the center.

S8. ANOTHER SET OF LINEAR FITTING DATA

Fig. S8 shows another independent set of the data by examining another single trapped particle when frequency f=3 MHz. A linear dependence of the rms fluctuation on $1/V$ is clearly seen. The reduced χ^2 value calculated from the linear fit in Fig. S8 is 0.26.

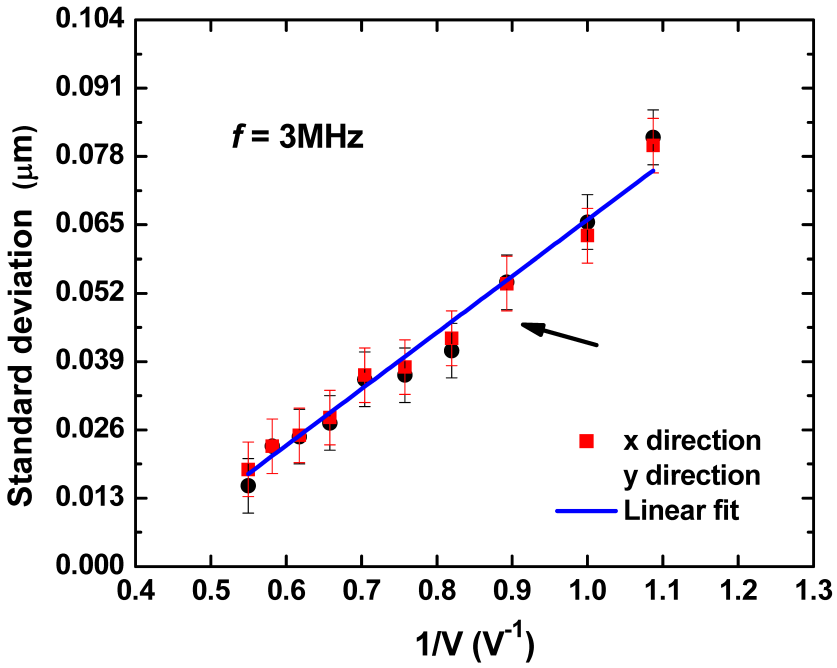

Figure S8. Dependence of the standard deviation of position fluctuations of a trapped bead on AC voltage at fixed frequency (3 MHz) for another independent experiment.

[S1] Duffy, D. C, McDonald, J. C, Schueller, O. J. A, & Whitesides, G. M. (1998) Rapid prototyping of microfluidic systems in poly(dimethylsiloxane). *Analytical Chemistry* **70**, 4974–4984.

[S2] Sbalzarini, I. F & Koumoutsakos, P. (2005) Feature point tracking and trajectory analysis for video imaging in cell biology. *Journal of Structural Biology* **151**, 182–195.

[S3] Wong, W. P & Halvorsen, K. (2006) The effect of integration time on fluctuation measurements: calibrating an optical trap in the presence of motion blur. *Optics Express* **14**, 12517–12531.

[S4] Henry, D. C. (1931) The cataphoresis of suspended particles. part i. the equation of cataphoresis. *Proceedings of the Royal Society of London. Series A* **133**, 106–129.

[S5] Ohshima, H, Healy, T. W, & White, L. R. (1983) Approximate analytic expressions for the electrophoretic mobility of spherical colloidal particles and the conductivity of their dilute suspensions. *Journal of the Chemical Society, Faraday Transactions 2* **79**, 1613–1628.

[S6] Palberg, Mnch, Bitzer, Piazza, & Bellini. (1995) Freezing transition for colloids with adjustable charge: A test of charge renormalization. *Physical Review Letters* **74**, 4555–4558.

[S7] Fiedler, S, Shirley, S. G, Schnelle, T, & Fuhr, G. (1998) Dielectrophoretic sorting of particles and cells in a microsystem. *Analytical chemistry* **70**, 1909–1915.

[S8] Muller, T, Gerardino, A, Schnelle, T, Shirley, S. G, Bordoni, F, DeGasperis, G, Leoni, R, & Fuhr, G. (1996) Trapping of micrometre and sub-micrometre particles by high-frequency electric fields and hydrodynamic forces. *Journal of Physics D: Applied Physics* **29**, 340–349.

[S9] Hughes, M. P & Morgan, H. (1998) Dielectrophoretic trapping of single sub-micrometre scale bioparticles. *Journal of Physics D: Applied Physics* **31**, 2205–2210.

[S10] Green, N. G & Morgan, H. (1999) Dielectrophoresis of submicrometer latex spheres. 1. experimental results. *Journal of Physical Chemistry B* **103**, 41–50.

[S11] Voldman, J, Braff, R. A, Toner, M, Gray, M. L, & Schmidt, M. A. (2001) Holding forces of single-particle dielectrophoretic traps. *Biophysical Journal* **80**, 531–541.

[S12] Pohl, H. A. (1978) *Dielectrophoresis: the behavior of neutral matter in nonuniform electric fields*. (Cambridge University Press.).

Supporting Information

Guan et al. 10.1073/pnas.1100977108

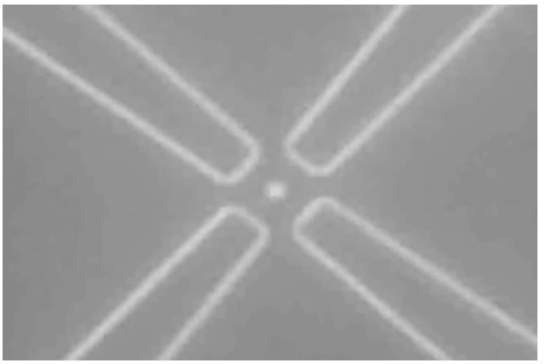

Movie S1. Typical dynamics of four basic operations: trapping with small fluctuations, trapping with large fluctuations, unstable trapping region (ejection), and resuming trapping.
Movie S1 (WMV)